Joint interpretation of seismic and CSEM data using well log constraints: an example from the Luva Field

One of the hottest trends in geophysical exploration today is the integration of data from multiple sources to produce a geologically consistent, quantitative interpretation of seafloor rock and fluid properties. In this case study Peter Harris,[1*] Zhijun Du,[2] Lucy MacGregor,[2] Wiebke Olsen,[1] Rone Shu[3] and Richard Cooper[3] present the application of a practical integration workflow to seismic, controlled source electromagnetic (CSEM), and well log data from the Luva gas field, offshore Norway.

Geophysical data are used routinely in exploration and reservoir characterization studies. However, when only a single data type is considered, ambiguities in the interpretation of the resulting data can remain. Seismic surveys are the most commonly used tool for surface based exploration of hydrocarbon resources. Seismic methods have evolved over the years and now provide high resolution images of the subsurface, which are used to develop geological models of structure and stratigraphy. Amplitude variation with offset (AVO) and inversion for acoustic and elastic impedance may also be used to constrain properties such as elastic moduli and density. However, despite the sophistication of seismic processing and interpretation methods, seismic data alone in many situations cannot give a complete picture of the reservoir. For example, AVO anomalies may be caused either by fluid or lithological variations, which cannot be separated on the basis of the seismic data alone.

The development of surface-based CSEM data allows us for the first time to complement high resolution structural and stratigraphic information from seismic data with surface-based resistivity measurements which can in some situations be directly related to the properties and distribution of fluids within subsurface structures. As with all remote sensing methods, ambiguities remain in the cause of the resistivity variations observed, particularly if these are interpreted in isolation. For example, a high resistivity anomaly may be caused by the presence of hydrocarbon, but could also be related to the presence of tight carbonates or volcanics.

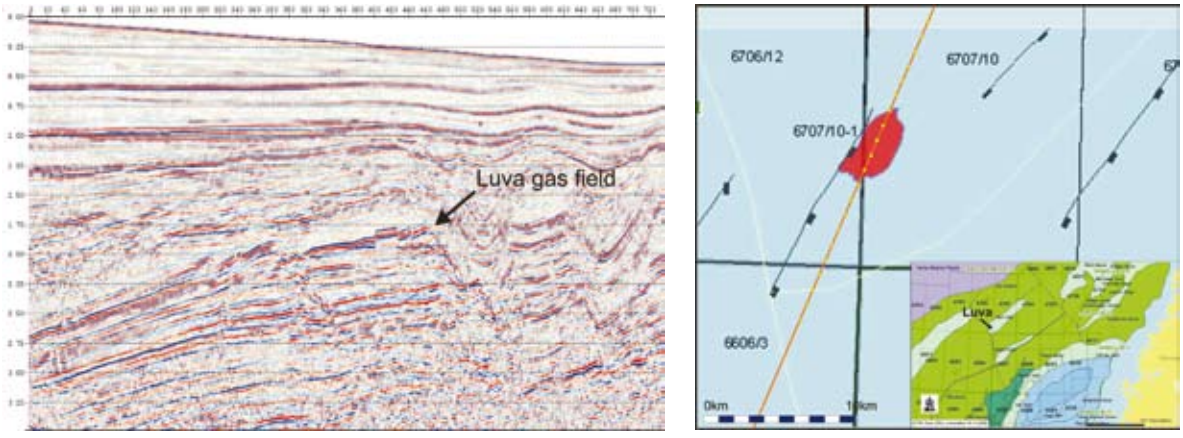

Figure 1 *Left panel: Seismic section through the Luva Gas field, located in the Nyk High, Voring Basin. The gas is trapped in a three-way dip closed structure bounded to the northwest by a fault. There is a pronounced flat spot indicating the gas-water contact. The gas sand is characterized by low acoustic impedance and high resistivity compared to surrounding strata. (Seismic data: courtesy TGSNopec). Right panel: The Luva CSEM survey used 21 receivers to record data. from a North-South trending source transmission line across the gas field. Note that the seismic and CSEM lines are not precisely coincident.*

[1] *Rock Solid Images, Oslo.*
[2] *OHM Aberdeen.*
[3] *Rock Solid Images, Houston.*
* *Corresponding author, E-mail: peter.harris@ohmrsi.com*

Well logs provide a high resolution measurement of the properties of a reservoir and the surrounding strata at the location of the well, and unlike seismic or CSEM data, log data can routinely provide information on rock and fluid properties. Logging tools use a variety of measurements, but within this suite of available log data, there is no more valuable indicator of fluid properties than the resistivity log. Indeed the integration of resistivity information with acoustic and other measurements is routine in petrophysical well log analysis.

The same integrated interpretation approach can be applied to remote sensing data, albeit at a very different scale and resolution. By integrating complementary sources of information in a consistent rock physics framework, and exploiting the strengths of each, estimates of rock and fluid properties such as gas saturation and porosity can be obtained with greater confidence than from any one data type alone.

In this paper we illustrate these ideas using seismic, CSEM, and well log data from the Luva gas field in the Norwegian sea. We first provide an overview of the CSEM acquisition and interpretation conditioned by structural information from the seismic, and follow that with a description of the well log based rock physics modelling. The log data that is used in the modelling is from the Norwegian Sea 6707-10-1 well (the Luva discovery). This well is located in the Nyk High, Vøring Basin, off the northwest coast of Norway in about 1274 m of water. The well has about 140 m of gas filled sand at about 3000 m total depth. Finally we illustrate a method of combining the inverted CSEM data with inverted seismic data through the rock physics models.

CSEM data

In 2006 OHM collected a CSEM survey across the Luva field, comprising 21 seafloor receivers, each recording two orthogonal electric field components, and a 41 km source transmission line over the receiver array. The fundamental transmission frequency was 0.25 Hz. Good quality electric field data were recovered from 18 of the 21 receivers deployed. Data processing resulted in amplitude and phase data (expressed as horizontal polarization ellipse (PE) parameters) extending to a maximum source-receiver separation of approximately 10 km in the fundamental frequency and 4–5 km in the higher harmonics.

Interpretation of CSEM data proceeds in stages, starting with simple approaches that provide a broad overview of the class of structures to which the data are sensitive, and gradually adds complexity. The first stage is to use 1D forward modelling and inversion on a receiver-by-receiver basis, and then combine the resulting resistivity structures to give a pseudo-section along the line. Details of the resistivity structure (such as the presence of localized resistive bodies) are unlikely to be constrained at this stage, which is designed to highlight larger scale variations in the background resistivity along the line.

Unlike seismic data, CSEM data in its native form cannot be used to make an image of earth structure. The primary tool used in the analysis of CSEM data is therefore geophysical inversion. Simply stated, the geophysical inversion process seeks an earth structure that is consistent with a measured dataset. However, it is well known that this process is non-unique and must be applied with care: given a finite, noisy dataset, an infinite number of structures can be found which can explain the data to a given level of misfit. In deterministic inversions this problem is addressed by regularization: constraints are placed on the class of structure that the inversion seeks.

This regularization can take many forms: for example, minimum norm regularization (the inversion seeks the model with the smallest 'size') is common in the inversion of EM data, as are derivative-based regularizations in which the derivative of model property with position is minimized.

If the first derivative is minimized then the model returned will be as close as possible to a uniform structure as is compatible with the data, whereas in the case of second derivative minimization, a model as close to a uniform gradient is sought.

The diffusive nature of EM fields means that measured data are not sensitive to the difference between sharp boundaries and more gradual changes in electrical properties. Derivative regularization is therefore appropriate since it matches the physics of the problem. However, inversion images resulting from fully regularized inversions of this sort are inherently smooth and fuzzy. Although unconstrained regularized inversion is therefore useful in that it illustrates the native sensitivity of the data to earth structure (only structure required by the data will be present in the inversion result), the resolution of structural detail is poor. A first stage in the integration process is therefore to use the structural information available from seismic data to condition and constrain the CSEM inversion process.

There are a number of approaches to this, which can be illustrated using a 1D synthetic example based on the structure of the Luva gas field (Figure 2), represented as a 140 m thick layer of resistivity 40 Ωm embedded in a uniform 2 Ωm background. The water depth is 1300 m. Synthetic data were generated assuming a source transmitting at 0.25 Hz, 0.75 Hz, and 1.25Hz (representing the fundamental, third and fifth harmonics of a square wave transmission signal), and a line of seafloor receivers in an inline geometry. The data were contaminated with 5% Gaussian noise, and signals below 10^{-15} V/Am^2 (corresponding to a typical noise floor in this water depth) were excluded from the dataset.

The effect of regularization and structural constraint can be investigated by inverting this synthetic dataset. Figure 3 shows the results of 1D inversion of the data using first derivative regularization, and a range of increasingly tight constraints. We use the Occam inversion algorithm described by Constable et al., 1987, and for each case the same uniform starting model was used in the inversion. The responses

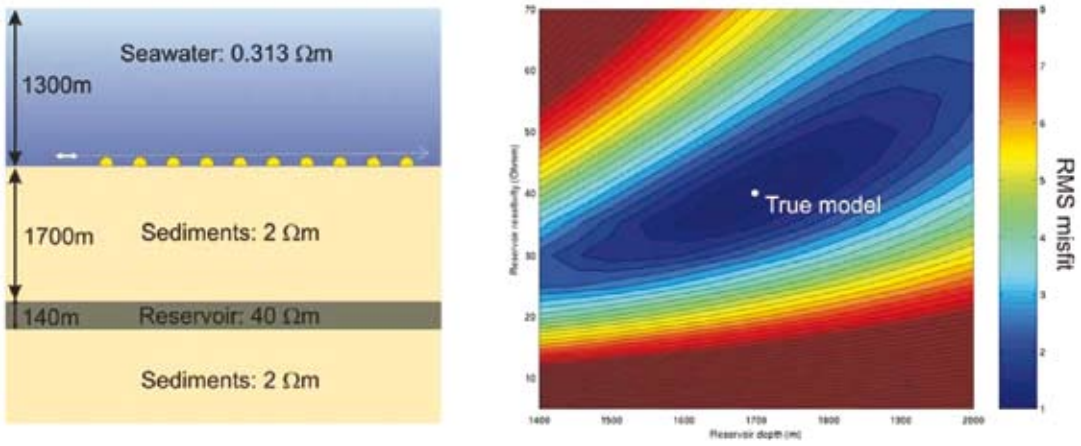

Figure 2 *Left panel: simplified 1D resistivity model based on the structure of the Luva gas reservoir. CSEM responses at 0.25 Hz, 0.75 Hz, and 1.25 Hz were contaminated with 5% noise to produce a synthetic dataset. Right panel: Misfit of the model response to the synthetic data as a function of target layer resistivity and depth. There is a clear trade off in these parameters.*

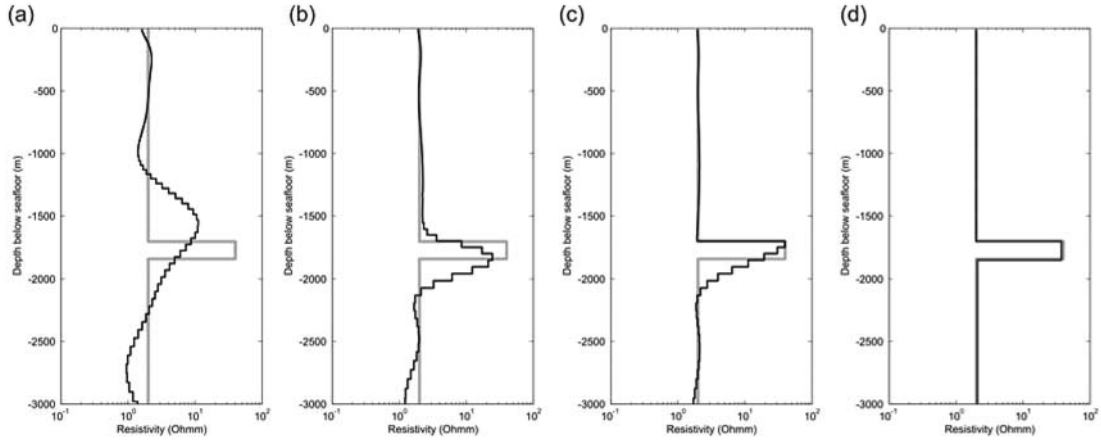

Figure 3 *(a) Result of unconstrained inversion of the synthetic dataset, using first derivative smoothing. The smooth model is consistent with the data but lacks structural detail. (b) Inversion with the resistivity from the seafloor to top reservoir prejudiced to the known background. (c) Inversion as for (b), but with a break in regularization at top reservoir allowing a sharp change in resistivity at this point. (d) As for (c), with a break in regularization at top and bottom reservoir. In each case the true model is shown in grey and the inversion result in black.*

to all these models fit the synthetic data to an RMS misfit level of 1.0 (the expected misfit in the presence of Gaussian noise), and are therefore equally valid models: mathematically there is nothing to choose between them. Figure 3a shows the result of unconstrained inversion of the data. This represents the smoothest model in the first derivative sense that is compatible with the observed data. Although there is a localized increase in resistivity resulting from the presence of the gas reservoir, it has a much lower resistivity than the true model, and is considerable shallower than the known depth of the target. Depth is often poorly constrained using CSEM data alone. This is illustrated in Figure 2b, where the misfit of the model response to the synthetic data as a function of reservoir depth and reservoir resistivity is plotted. There is a clear trade off in these parameters. A lower resistivity reservoir placed a few hundred metres shallower than the known reservoir depth will explain the data as well as the true reservoir model. An unconstrained inversion regularized in the first derivative sense will prefer the lower resistivity reservoir, since this minimizes the contrast with background resistivity and hence the vertical derivative. The result is a resistive zone corresponding to the reservoir but mapped too shallow.

In most practical situations we have seismic data in addition to the CSEM data and we can use this information to improve the resolution of the CSEM result by applying structural constraints based on the seismic data. This is illustrated in Figures 3b, c and d. In figure 3b we assume we know the depth of the reservoir interval. The resistivity in the overburden to this depth is prejudiced, by using a preferred background resistivity model, determined from well log analysis (if available) or careful modelling of off-structure CSEM data, to which the inversion will adhere if it is consistent with the input data (note that no values are

Structure	Transverse Resistance (Ωm^2)	Error Percentage
True model	5320	0
Unconstrained (Figure 5a)	3835	-28%
Figure 5b	4252	-20%
Figure 5c	5099	-4%
Figure 5d	5286	-1%

Table 1 *Percentage errors in transverse resistance derived from different inversions of synthetic data. Careful constraint on the inversion results in very low errors.*

fixed in this inversion approach). The result is still smooth, but the reservoir is placed at the correct depth.

The inversion result shown in Figure 3c is the same as that in 3b, with the addition of a break in regularization at the top of the reservoir (a sharp jump in resistivity is allowed at this point, which is assumed known from seismic or well information). This further improves recovery of the reservoir. Finally in Figure 3d, results are shown in which a break in regularization is allowed both at the top and base of the reservoir. In this case the resistivity structure of the initial model is extremely well resolved by the inversion.

The reservoir property that is best constrained by the CSEM method is the vertical integrated resistivity (known as the transverse resistance) of the reservoir. This simplifies to the resistivity thickness product for a simple 1D reservoir. The transverse resistance in the inversion results are shown in Table 1. The transverse resistance of the unconstrained inversion result is considerably lower than that of the true model, as a result of the non-uniqueness described above. However, the difference in the transverse resistance in the inversion result and true model falls to less than 5% when careful constraints are applied.

The principles above can be applied to the inversion of CSEM data from the Luva gas field. As in the synthetic case, data at three frequencies (0.25 Hz, 0.75 Hz ,and 1.25 Hz) were inverted, in this case for a two-dimensional resistivity structure. The overburden was prejudiced by a background resistivity structure derived from careful reconnaissance modelling of the off structure CSEM data. The result is shown in Figure 4. Also shown in Figure 4 is a pseudo well extracted from the inversion. Once the depth to the reservoir is constrained, the resistivity of the gas field can be obtained accurately from the CSEM data.

Rock physics modelling

At the heart of any integrated interpretation approach is a consistent rock physics framework that allows both electric and elastic properties of a medium to be calculated from its lithology and fluid properties. Using data from 6707/10-1 we can construct and validate acoustic and electric rock physics models for the Luva field. These are then used in the first stage of the seismic and CSEM integration study, which involves fluid substitution and modelling, and serves as a feasibility check on our ability to discriminate gas-filled from wet sands. In addition, it is used to help calibrate and interpret the results. Figure 5 shows the smoothed well log data and the modelled gas sand zone.

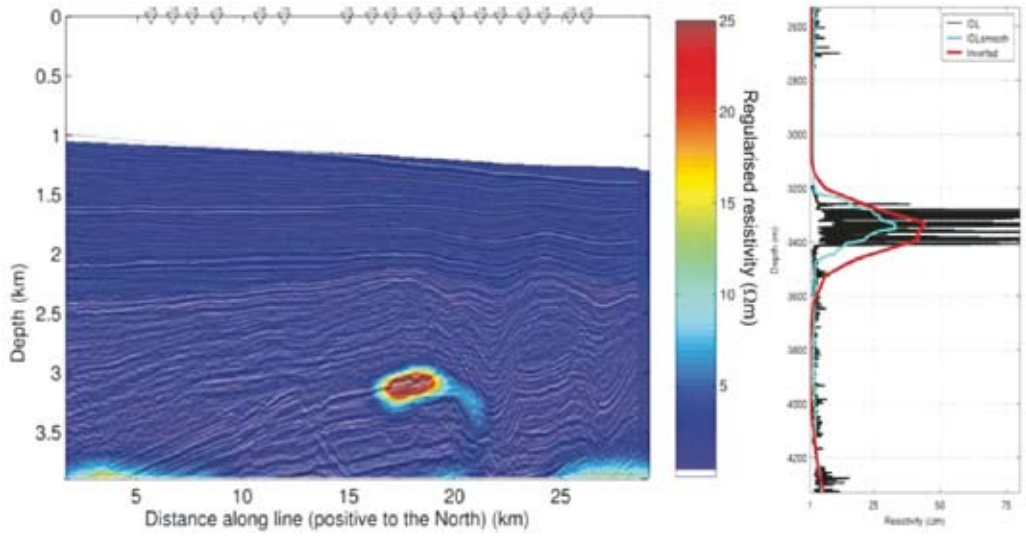

Figure 4 *Left panel: Constrained inversion of CSEM data from the Luva Gas field. By including structural constraints from the seismic data, along with careful analysis of overburden structure, the resolution of the resistivity image of the reservoir can be improved. Right panel: Pseudo-well extracted from the CSEM inversion result (red), compared to the resistivity from well log data (black) and a smoothed well log curve (blue). Electrical properties of the reservoir can be more accurately recovered when appropriate constraints are placed on the inversion.*

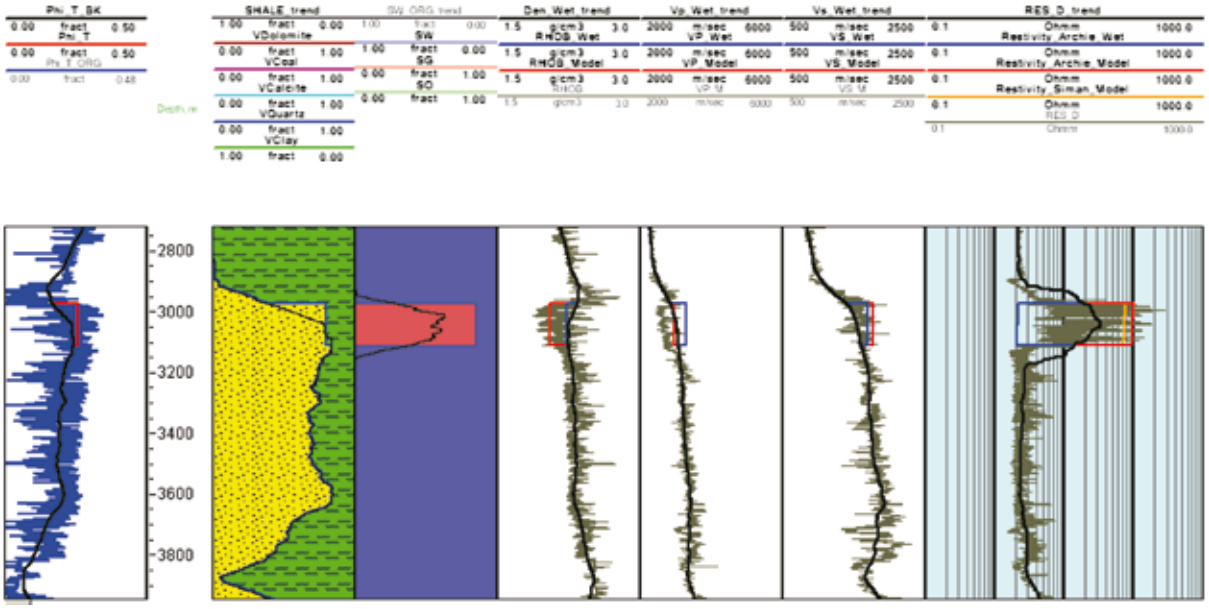

Figure 5 *Fine scale (grey) and smoothed (black) well log curves (6707-10-1 well) and modelled gas sand at about 3000 m depth.*

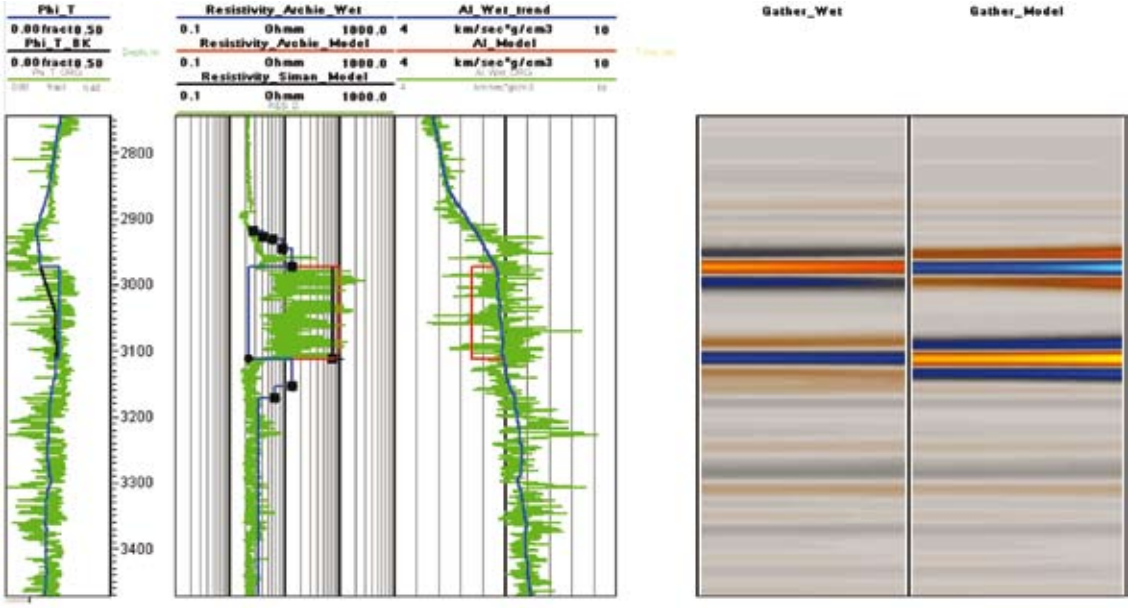

Figure 6 *Synthetic seismic gathers show strong amplitude difference between wet case (left) and 85% gas case (right). Orange colours in the gather indicate positive amplitude (low AI over high AI), blue colour indicates negative amplitude (high AI over low AI).*

The first step in modelling is to compute the seismic AVA and 1D CSEM responses in-situ and in 100% water saturated conditions. If these models show substantial differences between gas and wet cases, then we have an important indication that hydrocarbon detection is feasible. The average in-situ gas saturation in the pay sand is about 85%, so our initial model will represent the 85% Sg case. As shown in Figure 6, there is a substantial difference between the wet and 85% gas synthetic gathers. In the wet case, the top of the sand has positive amplitude (high impedance) but, in the gas case, we see negative amplitude (low impedance). We used Biot-Gassmann to compute the seismic velocity changes. Electrical resistivity changes were computed for clean sand and shaly sand cases using Archie and Simandoux models respectively (Mavko, et al., 2003). Seismic gathers were computed using a 30 Hz Ricker wavelet and the CSEM frequency was 1 Hz.

The relative effects of high gas saturation (85%) are shown in Figure 7 for both the seismic AVA method and the CSEM method. Note that for seismic response we see a

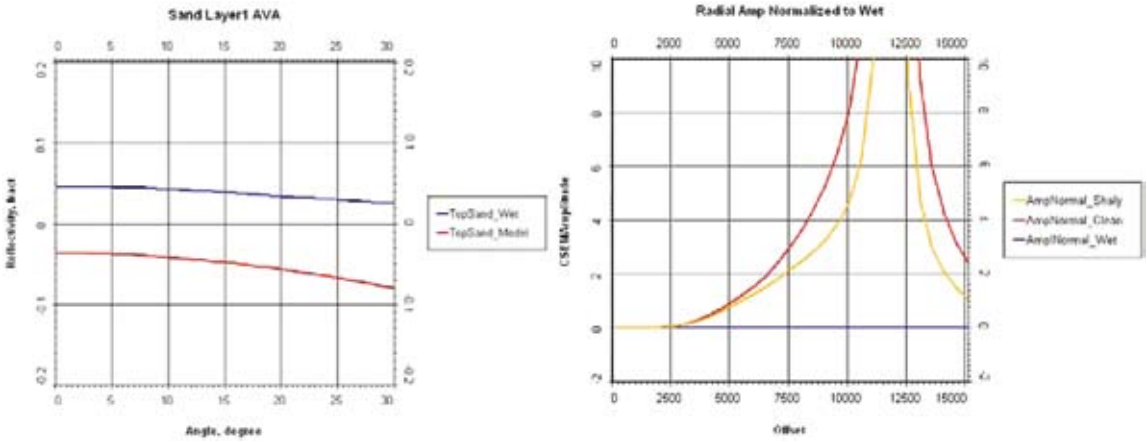

Figure 7 *(left) Reflectivity versus angle of incidence for wet (blue line) and 85% gas case (red line); (right) Normalized radial CSEM amplitude versus source-receiver distance for wet (base case) and 85% gas case. Note that the difference between the wet and gas case CSEM amplitude ranges from a factor of five for shaly sand (orange line) to a factor of eight for clean sand (red line) at the maximum spacing of 10,000 m.*

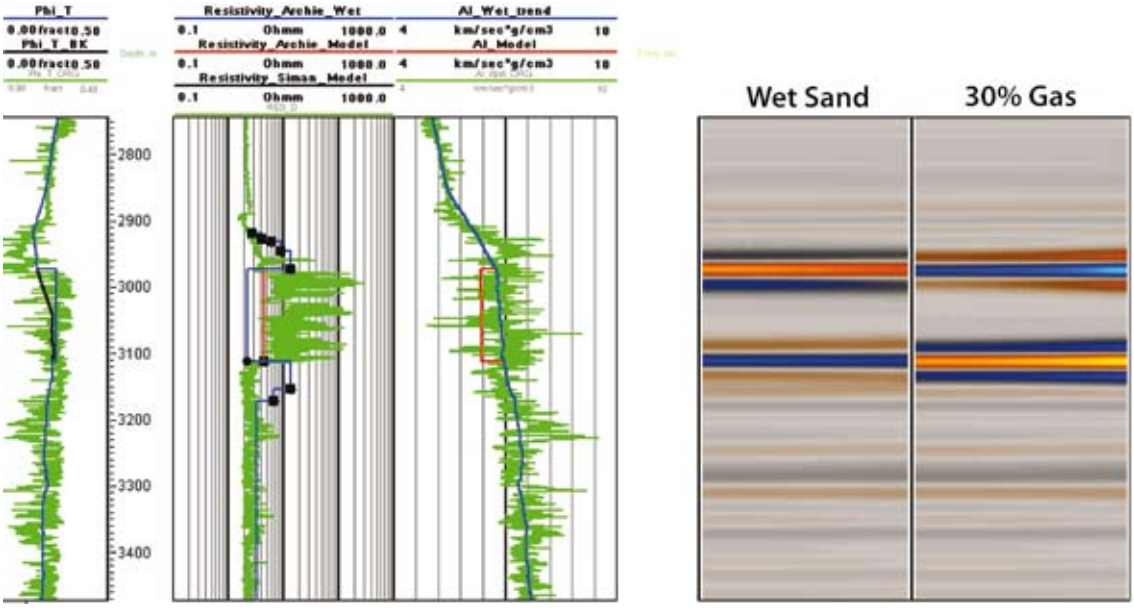

Figure 8 *Synthetic seismic gathers show strong amplitude difference between wet case (left) and the non-commercial 30% gas case (right).*

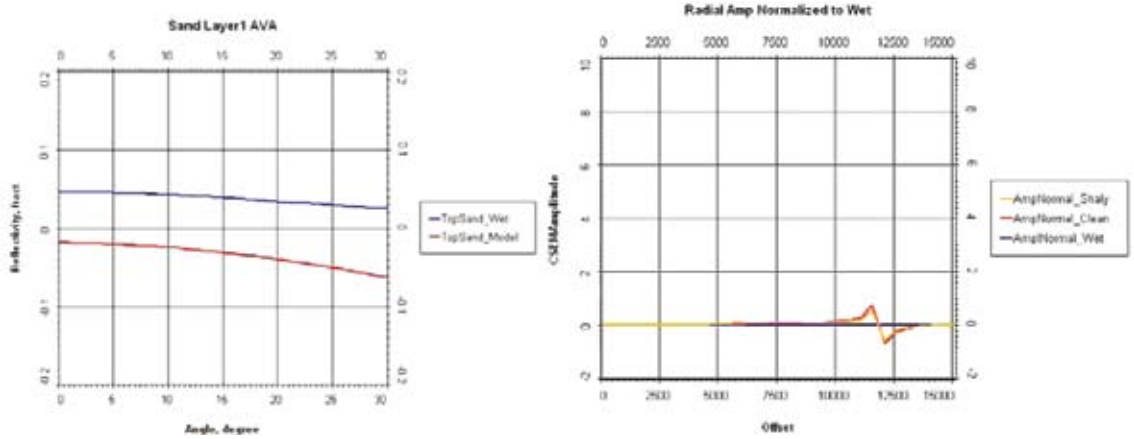

Figure 9 *(left) Reflectivity versus angle of incidence for wet (blue line) and 85% gas case (red line); (right) natural log of normalized radial CSEM amplitude versus source-receiver distance for wet and 30% gas case.*

change in reflectivity polarity when water is replaced by gas in the reservoir. The CSEM plot shows substantially higher amplitude for the gas case that peaks at about 10,000 m total offset (where for this dataset the signal falls below the 10^{-15} V/Am^2 noise floor); however, significant and measureable CSEM responses would be observed (for this 1D case) at ranges greater than 4–5 km.

The next set of models show the effect on seismic AVA and CSEM response for the case where gas saturation in the sand is measurable, but not commercially viable. Figure 8 shows the synthetic seismic gathers for the wet case and the 30% gas case. The non-commercial 30% gas case on the right is almost identical to the 85% gas case gather in Figure 6. Note also that the seismic AVA crossplot on the left side of Figure 9 shows that the effect of 30% gas is about the same as the effect of 85% gas, shown in Figure 7. However, the CSEM data (right side of Figure 9) for 30% gas exhibits a very substantial difference from the 85% gas case in Figure 7.

Based on these models, we conclude that prestack seismic gathers alone cannot discriminate low gas saturation from high gas saturation in this case. However, if CSEM data are available at this location, then we have a very sensitive indication of the commercial versus non-commercial gas concentration. It is interesting to note further that the CSEM data here cannot distinguish between the water wet case and the low gas saturation case, although the seismic data are very sensitive to such a change (Walls et al., 2008).

Seismic inversion

We used 2D seismic data acquired by TGS-Nopec as the basis for the inversion. They were of generally good quality, but nonetheless we applied a data conditioning sequence to the pre- STM gathers before inversion. Such conditioning can be shown to dramatically improve the quality and robustness of the inversion result (Singleton, 2009) . The conditioning sequence consisted of

- Residual multiple attenuation, using a high resolution Radon transform.
- Residual moveout correction.
- Spectral balancing across offsets, to ensure that the wavelet is reasonably stationary with offset.
- Random noise removal, using a 3D edge-preserving filter on offset cubes.

The data conditioning addresses the main issues of data quality that we frequently see in prestack time migration gathers and makes them fit for AVO inversion. The seismic inversion was performed on our angle stacks created by stacking over the ranges of incidence angles 2°–10°, 10°–18°, 18°–26°, and 26°–35°. The inversion algorithm itself is described by Tonellot (2001) and is based on standard approximations to the Zoeppritz equations. It allows constraints on lateral smoothness in the solutions, and has explicit control over the relative influence of the data and the initial model in the results, which are determined by estimating the signal-to-noise ratio of the data and misfit values of the initial model at well locations. The initial model is constructed by

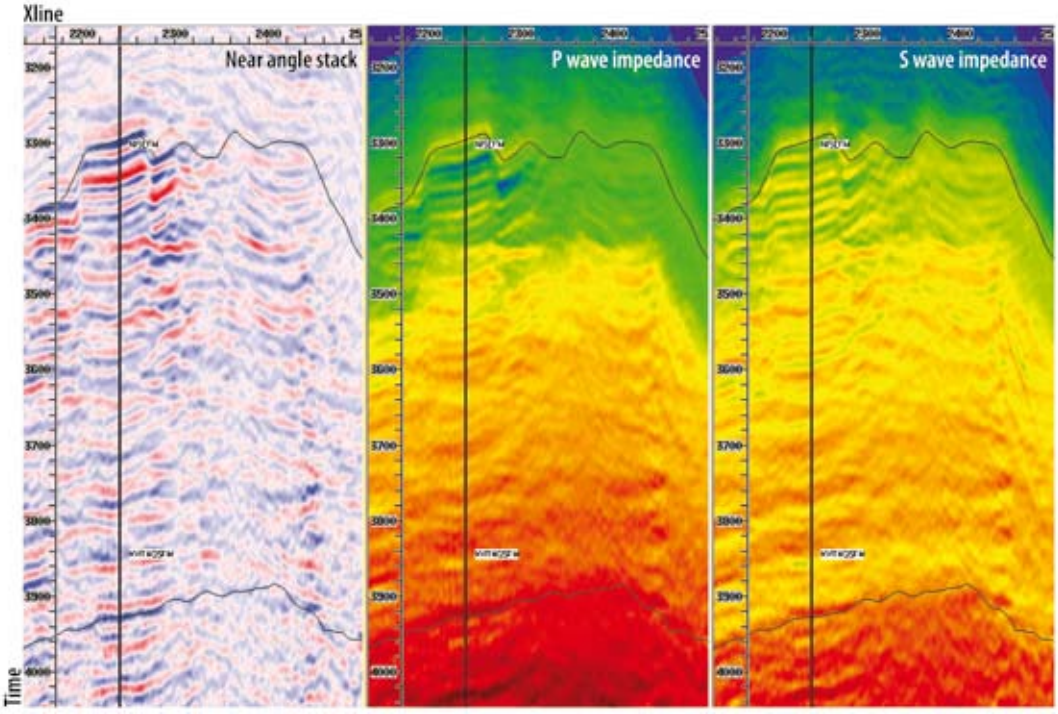

Figure 10 *from left to right: Near angle stack, P wave impedance, S wave impedance. The top reservoir pick and the well location are also shown. The gas-water contact is evident in the seismic data and is brought out clearly as the green-yellow transition in the P wave impedance.*

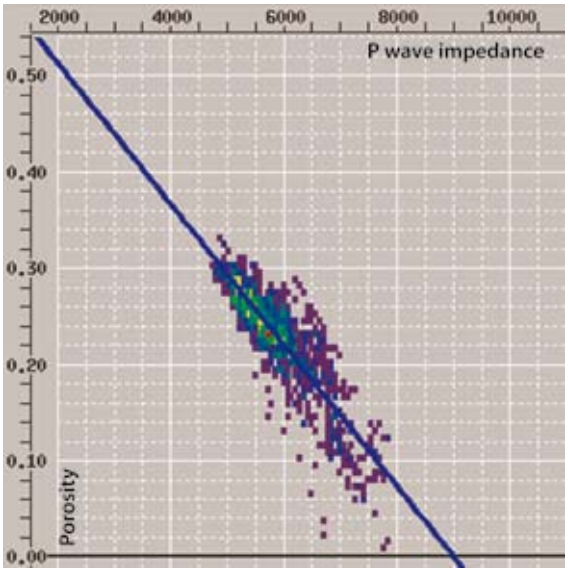

Figure 11 *Crossplot of porosity versus P wave impedance for the reservoir interval. There is a well-defined linear relationship in the reservoir unit.*

smoothing the P velocity, S velocity, and density logs by Backus averaging over a moving window, followed by horizon-guided interpolation via co-kriging between wells.

A stack, together with the P wave impedance and the S wave impedance from the inversion, are shown in Figure 10. There is a clear flat spot and it is easy to pick the top reservoir reflection. However, it is evident that within the main fault block there are non-producing shale intervals. These are very clear in the logs, and the two thickest ones are also visible in the seismic data. A crossplot of P wave impedance versus S wave impedance allows us to identify the shales at the well location, and this classification is extended to the rest of the seismic data within the top-base reservoir picks. The seismically non-resolvable shales remain unclassified, thus contributing to uncertainty in our reservoir property estimates.

Combining seismic, CSEM and well data

Having inverted both the seismic and CSEM data to obtain images of impedence and resistivity respectively, the final stage in the process is to apply well log derived calibrations to these results to provide estimates of the rock and fluid properties of the reservoir. The well logs indicate a straightforward linear relationship between porosity and P wave impedance within the reservoir interval (Figure 11), which seems to be largely independent of lithology. Upscaling these with a running Backus average of velocities and density over a 12 m interval, and using an arithmetic running average of porosity produces a small change in the linear relationship. Thus we feel comfortable using the relationship as a direct mapping between P wave impedance and porosity.

As we have seen, the relationship between resistivity and gas saturation is complicated by the presence of the non-resolvable shales. This contributes to the uncertainty in gas saturation estimates from the inverted CSEM resistivity. We therefore find it more useful to produce upper and lower bounds on gas

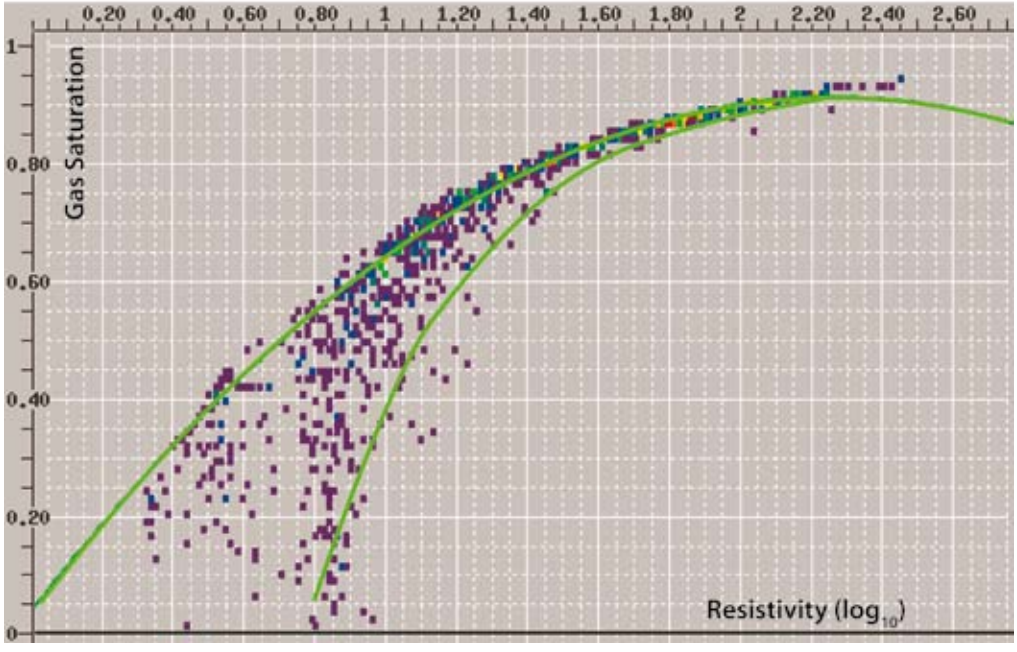

Figure 12 *Gas saturation versus log10(resistivity). The green line represents an upper bound on the gas saturation, and equally well a lower bound can be obtained from the lower limit of the point cloud. The scatter between them is partly due to the varying clay content within the reservoir sands. At high saturations the uncertainty in the saturation estimate is low, whereas at lower saturations it becomes greater.*

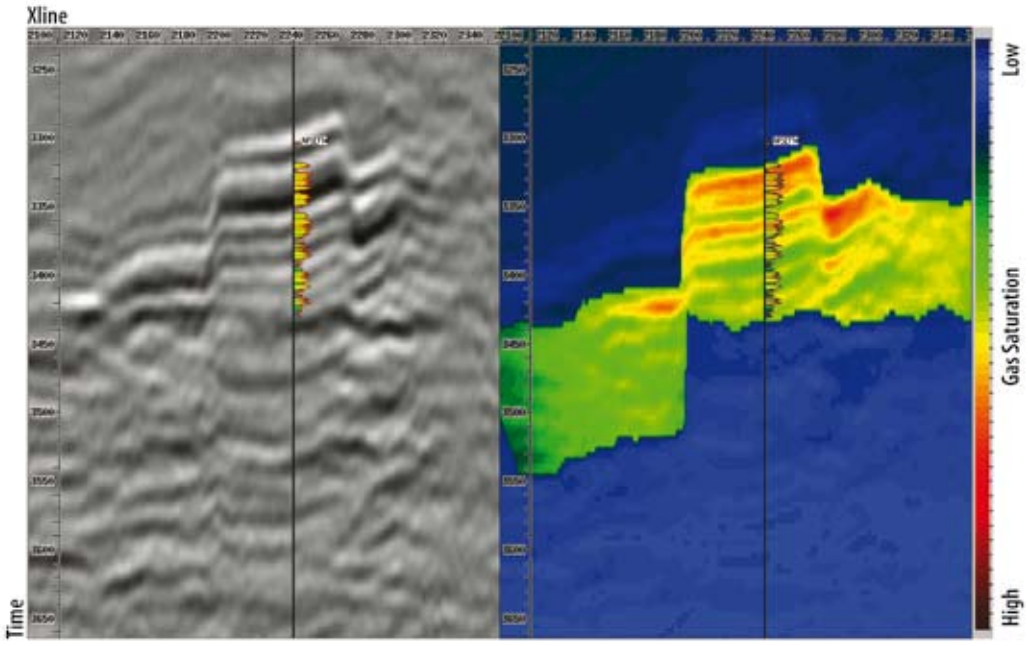

Figure 13 *Left, near angle stack of the seismic data, with the gas volume (porosity times gas saturation) log superimposed. Although the seismic image shows the reservoir structure in some detail, it does not, by itself, provide information on the fluid content. Right, gas volume section derived from the combined CSEM and seismic inversions. The low saturation shales stand out clearly as the darker green events within the reservoir unit. The highest gas volume lies at the top of the reservoir, as expected.*

saturation, based on the crossplot (Figure 12). As these data include the shale influence, the bounds are considered reliable.

Due to the relatively low vertical resolution of the resistivity section, the gas saturation estimate is considered as an average over the reservoir interval. However, the gas volume (porosity times saturation) is a clearer indicator of the structure of the vertical gas distribution. In Figure 13 it is evident that the highest concentration of gas lies in the upper section of the reservoir interval and that the intra-reservoir shales are identified.

Discussion

In many instances the demands of reservoir characterization go beyond simple images of structure, impedance and resistivity: quantitative estimates of lithology and fluid properties are required to fully understand the character of a field. Here, we have presented an approach to integrating seismic and CSEM data that permits estimates beyond those obtainable from just one type of data.

Understanding the rock physics underlying the electric and elastic properties measured, and developing a consistent description of rock properties is the key to successful integration, and requires the use of well information. Specific details are of course field and lithology dependent, but we generally find that, as in this case, the P wave impedance contains most of the porosity information and that the resistivity is the most useful measurement for fluid saturation. Lithology identification and shale content are less clear cut, and often P impedance, S impedance, and resistivity are all required to obtain reasonable estimates of shaliness. Without these estimates, the saturation results are likely to be biased by the presence of clay minerals within reservoir sands, as the clay minerals have a strong influence on the resistivity.

Both resolution and the problem of correct depth registration of the different data types have to be addressed in some detail for the joint interpretation to be successful. It is therefore essential to have well information for depth registration by checking both seismic and CSEM well-ties.

Acknowledgements

Much of this work was carried out within the industry-funded WISE Consortium. We thank the sponsors, BERR, Chevron, DONG E&P, Maersk Olje og Gas, Det norske, and Total for their support. We are grateful to TGS-Nopec for allowing us to show the seismic data.

References

Constable, S., Parker, R. and Constable C. [1987] Occam's inversion: A practical algorithm for generating smooth models from electromagnetic sounding data. *Geophysics*, **52**, 289-300.

Mavko, G., Mukerji, T. and Dvorkin, J. [2003] *The Rock Physics Handbook*. Cambridge University Press.

Singleton, S. [2009] The effects of seismic data conditioning on pre-stack simultaneous impedence inversion. *The Leading Edge*, in press.

Tonellot, T., Mace, D. and Richard, V. [2001] Joint Stratigraphic Inversion of Angle-Limited Stacks. *SEG Annual Meeting*, Expanded Abstracts, **20**, 227.

Walls, J. and Shu, R. [2008] Seismic and EM rock physics and modelling, Norwegian Sea. *SEG Annual Meeting*, Expanded Abstracts, **27**, 657.